RSC Advances

PAPER

View Article Online
View Journal | View Issue

Cite this: *RSC Adv.*, 2016, **6**, 26559

Impact of neutral and anion anchoring groups on the photovoltaic performance of triphenylamine sensitizers for dye-sensitized solar cells†

Thogiti Suresh,[a] Ramesh Kumar Chitumalla,[b] Nguyen Thi Hai,[a] Joonkyung Jang,[b] Tae Jin Lee*[a] and Jae Hong Kim*[a]

Received 8th January 2016
Accepted 1st March 2016

DOI: 10.1039/c6ra00636a

www.rsc.org/advances

Anchor groups play a vital role in dye-sensitized solar cells (DSSCs), acting as a bridge for electron injection from the sensitizers to the metal oxide semiconductor. Carboxylic acids (COOH) are widely used anchors for most sensitizers because of their strong adhesion to the semiconductor surface. Electron injection occurs through this adhesion, which is the main process that initiates the electrical circuit in a DSSC. Owing to the proton (H^+) of the COOH anchoring group, the conduction band of the semiconductor is shifted positively after sensitizer adsorption, leading to open circuit photovoltage (V_{OC}) loss. In this study, the triphenylamine-based sensitizer with a carboxylate group (COO^-) was synthesized as an anchor. Although the power conversion efficiency of the anionic triphenylamine sensitized solar cells was lower than that of the neutral-base cell due to the decreased amount of dye on the photoelectrode surface, it exhibited an enhanced V_{OC} compared to that of the neutral form. Density functional theory (DFT) and time dependent DFT studies were also carried out to theoretically characterize the two dyes and explore the difference between the carboxylic and carboxylate anchor groups.

1. Introduction

Dye-sensitized solar cells (DSSCs) are a promising alternative to conventional p–n junction solar cells because of their low cost and flexible fabrication.[1–4] To date, some cells with ruthenium complexes as dye sensitizers have achieved power conversion efficiencies (PCEs) of more than 11%.[5,6] Moreover, the zinc–porphyrin-sensitized DSSCs have reached an efficiency of more than 12%.[7,8] On the other hand, regarding the limited ruthenium resources and the purification difficulty for zinc–porphyrin dyes, metal-free organic dyes have attracted increasing attention because of their advantages over metal sensitizers. The advantages are due to their environment friendly, high molar extinction coefficient, tunable molecular energy level, cost-effectiveness, and inexpensive syntheses by using well-known synthetic methodologies and they show optical, electronic, and electrochemical properties that can be modified through appropriate molecular engineering.[9–15] Most metal-free organic sensitizers are designed with the donor–π–acceptor structures, which are comprised of an electron donor, a conjugated linker and an electron acceptor/anchor. The most popular acceptor/anchor is cyanoacrylic acid, which contains the electron withdrawing properties of the cyano group (C≡N) and an anchor carboxylic acid group (COOH). The strong electron acceptor cyano group and strong anchor COOH group lead to easy electron extraction from the excited sensitizer to the conduction band of the metal oxide semiconductor as well as an enhanced dye loading on the metal oxide semiconductor, which increases the photovoltaic performance of DSSCs compared to other acceptors/anchors.[16] Recently, most studies used cyanoacrylic acid in the neutral form of the carboxylic acid (COOH), which gives a proton on the metal oxide semiconductor surface after dye adsorption, leading to a positive shift in the conduction band of the semiconductor, resulting in open circuit photovoltage (V_{OC}) loss. It is well-known that the adsorption mode has a significant influence on photovoltaic parameters of DSSC such as the open circuit voltage and short circuit current.[12–21] Utilizing COOH as anchoring group, the binding modes with a semiconductor surface might be mono-dentate or bi-dentate. Between the two binding modes, bi-dentate binding exhibits stronger attachment and more effective electron injection than mono-dentate binding.[17]

In 2013, Zhang *et al.* tried to add water to the electrolyte to change the pK_a of the carboxyl group, which promotes the deprotonation of the carboxyl group, leading to a change from mono-dentate to the bi-dentate binding of the Eosin Y sensitizer

[a]*Department of Chemical Engineering, Yeungnam University, 214-1, Dae-dong, Gyeongsan, Gyeongbuk 712-749, Republic of Korea. E-mail: jaehkim@ynu.ac.kr; tjlee@ynu.ac.kr*

[b]*Department of Nanoenergy Engineering, Pusan National University, Busan, 609-735, Republic of Korea*

† Electronic supplementary information (ESI) available. See DOI: 10.1039/c6ra00636a

on TiO_2 surface to increase the efficiency.[17] In 2015, Bao *et al.* synthesized julolidine based neutral and anion anchoring dyes and concluded that the anion anchoring dye is beneficial to electron injection, which improves open circuit-voltage, short circuit current and overall power conversion efficiency.[22] Conventionally, the deprotonated anchor is regarded as being more stable than the protonated anchor.[23] Therefore, investigation of the protonation/deprotonation of dye carboxyl anchor is still important.

This paper reports the synthesis of the 3-{5-[4-(bis-{4-[5-(2-carboxy-2-cyano-vinyl)-thiophen-2-yl]-phenyl}-amino)-phenyl]-thiophen-2-yl}-2-cyano-acrylate (anion TPA3T3A)-based sensitizer with carboxylate group (COO^-) as an anchor. The anion TPA3T3A sensitizer is identified by nuclear magnetic resonance (NMR) spectroscopy and Fourier transform infrared (FT-IR) spectroscopy compared to the neutral TPA3T3A sensitizer. Anion TPA3T3A does not contain a proton, which maintains the TiO_2 conduction band level, thereby increasing V_{OC} compared to the performance of the neutral form. Moreover, the absorption binding of the anion TPA3T3A to the TiO_2 surface is bi-dentate, whereas the neutral form shows both mono-dentate and bi-dentate binding, which leads to more surface coverage of the anion form, resulting in a reduced recombination rate from the TiO_2 surface and oxidized-electrolyte insulation.[24] This paper reports a new strategy for enhancing the performance of DSSCs using ion sensitizers. The experimental UV-visible absorption spectra are compared with the theoretically obtained UV-visible spectra. The electron density distribution of the dyes in their frontier molecular orbitals is obtained using density functional theory (DFT).

2. Experimental section

2.1 Materials and instruments

All starting materials and solvents were purchased from Aldrich and used as received. All ^{1}H-NMR spectra were measured on a Bruker Advance NMR 300 MHz spectrometer using DMSO-d_6. The FT-IR spectra were recorded using a Perkin Elmer Fourier Transform Infrared (FT-IR) spectrometer. The UV-vis absorption of the dye solutions and dye absorbed TiO_2 films were examined using a Cary 5000 UV-vis-NIR spectrophotometer. The active areas of the dye-adsorbed TiO_2 films were estimated using a digital microscope camera with image-analysis-software (Moticam 1000, Motic). The film thickness was measured using an Alpha-step IQ surface profiler (KLA Tencor). Electrostatic deposition was conducted using a DC supply (MCP DC Power Supply M10-QS 305).

2.2 Synthesis

The TPA3T3A neutral form was prepared using the synthesis method reported elsewhere.[25] ^{1}H-NMR (300 MHz, DMSO-d_6): δ 8.480 (s, 3H), 8.016 (d, $J = 3.9$ Hz, 3H), 7.790 (d, $J = 8.4$ Hz, 6H), 7.720 (d, $J = 3.9$ Hz, 3H), 7.213 (d, $J = 8.4$ Hz, 6H).

The TPA3T3A anion form was obtained by dehydrogenation of the TPA3T3A neutral form by silica gel column chromatography with methanol as the eluent. ^{1}H-NMR (300 MHz, DMSO-d_6): δ 7.987 (s, 3H), 7.69 (d, $J = 8.4$ Hz, 6H), 7.648 (d, $J = 3.9$ Hz, 3H), 7.534 (d, $J = 3.9$ Hz, 3H), 7.157 (d, $J = 8.4$ Hz, 6H).

2.3 DSSCs fabrication and photovoltaic performance measurements

A cleaned fluorine-doped tin oxide (FTO) transparent conducting glass substrate (Pilkington, 15 Ω cm^{-2}) was coated with transparent TiO_2 paste (20–30 nm in diameter, Dyesol Ltd.) using the doctor blade technique, followed by sintering at 450 °C for 30 min. The TiO_2 particles as the scattering layer (200 nm in diameter, Dyesol Ltd.) were then deposited onto the transparent TiO_2 films, followed by sintering at 450 °C for 30 min. Two layers of TiO_2 films were treated with a 40 mM aqueous $TiCl_4$ solution at 70 °C for 30 min and then sintered at 450 °C for 30 min. After cooling to approximately 80 °C, the TiO_2 films were immersed in the neutral and anion TPA3T3A solutions (0.3 mM) at 25 °C for 24 hours in the dark, and the residual dye was rinsed off with acetonitrile to give the working electrode. The counter electrodes were prepared by depositing platinum paste onto the FTO glasses using the doctor blade technique, followed by sintering at 450 °C for 30 min. The working electrode and Pt counter electrodes were sealed with a 60 μm thick Surlyn film (Dupont), and filled with the electrolyte solution through pre-drilled holes on the Pt counter electrode. The electrolyte solution consisted of 1-butyl-3-methylimidazolium iodide (0.7 M), lithium iodide (LiI, 0.2 M), iodine (I_2, 0.05 M) and *t*-butylpyridine (TBP, 0.5 M) in acetonitrile/valeronitrile (85 : 15, v/v). The photo current density–voltage (*J*–*V*) characteristics of the prepared DSSCs were measured under AM 1.5 irradiation with an incident power of 100 mW cm^{-2} (PEC-L11, Peccell Technologies, Inc.). The incident monochromatic photon-to-current efficiencies (IPCEs) were recorded as a function of the light wavelength using an IPCE measurement instrument (PEC-S20, Peccell Technologies, Inc.). Electrochemical impedance spectroscopy (EIS) was carried out with a computer-controlled potentiostat (IVIUMSTAT, IVIUM) at the open circuit voltage with a 10 mV amplitude and an AC frequency ranging from 100 kHz to 0.1 Hz (PEC-L11, Peccell Technologies, Inc.).

2.4 Computational details

All the DFT/TDDFT calculations reported in this paper were carried out using the Gaussian 09 *ab initio* quantum chemical program.[26] The ground-state geometry optimization was carried out by the hybrid exchange (25%) and correlation (75%) functional PBE0 (ref. 27 and 28) coupled with the 6-311G(d,p) basis set. At the same level of theory, the frequency calculations were carried out to confirm the nature of the minima obtained on the potential energy surface. The UV-visible spectra of the dyes were obtained using TDDFT formalism. In the TDDFT simulations, the CAM-B3LYP[29] long range corrected functional and 6-311G(d,p) basis set was used. The polarizable continuum model[30] was used in TDDFT simulations to account for the solvent (*N*,*N*-dimethylformamide) effects.

3. Results and discussion

3.1 Structure identification of neutral and anion based dye sensitizers

In this study, the TPA3T3A sensitizer was modified with the D–π–A structure using the triphenylamine unit as an electron donor, the thiophene unit as the bridge and cyanoacrylic acid unit as the acceptor/anchor. TPA3T3A exhibited the neutral and anion form based on the neutral form of the carboxylic COOH group and the anion form of carboxylate COO^- group, Fig. 1. Anion TPA3A3T was obtained by neutral TPA3T3A dehydrogenation using silica gel column chromatography with methanol as the eluent. To identify the existence of the neutral and anion TPA3T3A, the ^1H NMR spectra were recorded in DMSO-d_6 solvent (Fig. S1 and S2†). The two forms could be distinguished by observing the presence of a hydrogen peak in carboxylic acid (COOH) around 11–12 ppm. On the other hand, carboxylic hydrogen occurs as a broad singlet peak that cannot be observed due to chemical exchange of the substance with the solvent DMSO-d_6 in solution. Therefore, to demonstrate the presence of the neutral and anion form, the chemical shift of 5 other hydrogen types needs to be investigated. Fig. 1 shows that all the corresponding hydrogens of neutral TPA3T3A are shifted downfield compared to anion TPA3T3A because the electron withdrawing effect of the carboxylic acid group is stronger than that of the carboxylate group.

FT-IR spectroscopy of the neutral and anion TPA3T3A in the solid state is performed for further confirmation (Fig. 2). The main signals are recognized in the following wavelength range: the free carboxyl groups (C=O) shows a signal at 1700–1730 cm^{-1}; symmetric and asymmetric COO^- group are found at 1420–1450 cm^{-1} and 1550–1600 cm^{-1}, respectively; and the stretching of C≡N appears at 2200–2300 cm^{-1}.[17] In the case of anion TPA3T3A, the electronic arrangement is stabilized by electron delocalization to establish a resonance structure; thus the carbonyl bond (C=O) is considered to have disappeared. As shown in Fig. 2, the signal for free carbonyl group in anion TPA3T3A is not observed in range, 1700–1740 cm^{-1}, but the peak for carbonyl bonding of neutral TPA3T3A is observed strongly at 1713 cm^{-1}.

3.2 Optical properties of neutral and anion dyes

Fig. 3 presents the UV-vis absorption spectra of the neutral and anion TPA3T3A in DMF and absorbed on the TiO_2 thin films. The absorption band of the anion TPA3T3A solution appeared at approximately 375–500 nm with the maximum absorption wavelength (λ_{max}) at 429 nm and a molar extinction coefficient (ε_{max}) of 7.12 × 10^4 M^{-1} cm^{-1}, whereas the neutral TPA3T3A solution exhibited a broader and red shifted absorption band from 375–550 nm with a maximum absorption wavelength at λ_{max} = 441 nm ($\Delta\lambda_{max}$ = 12 nm) and

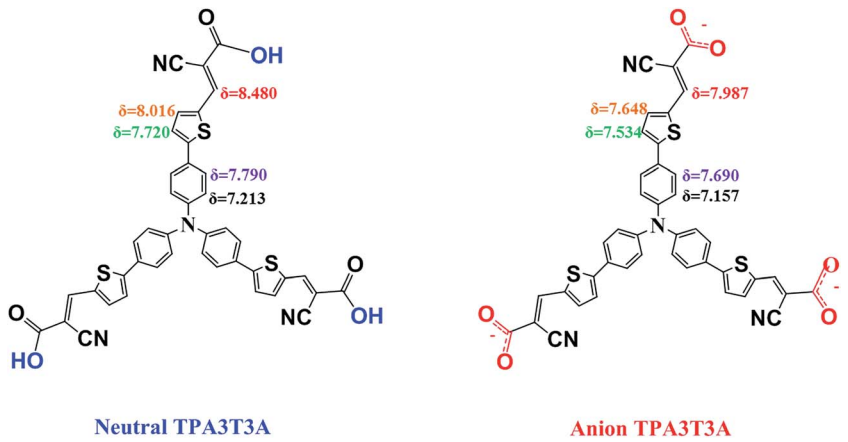

Fig. 1 Molecular structure and ^1H NMR chemical shift of each corresponding hydrogen of neutral and anion TPA3T3A.

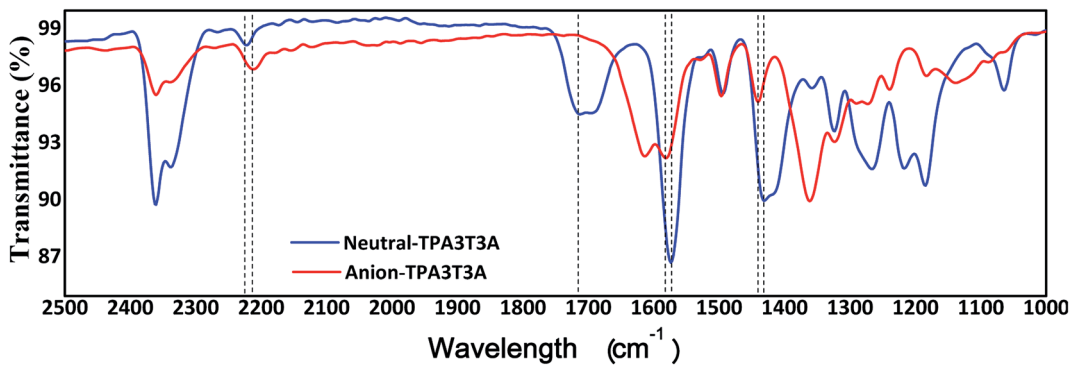

Fig. 2 FTIR spectra of solid neutral and anion TPA3T3A over the wavelength range, 1000–2500 cm^{-1}.

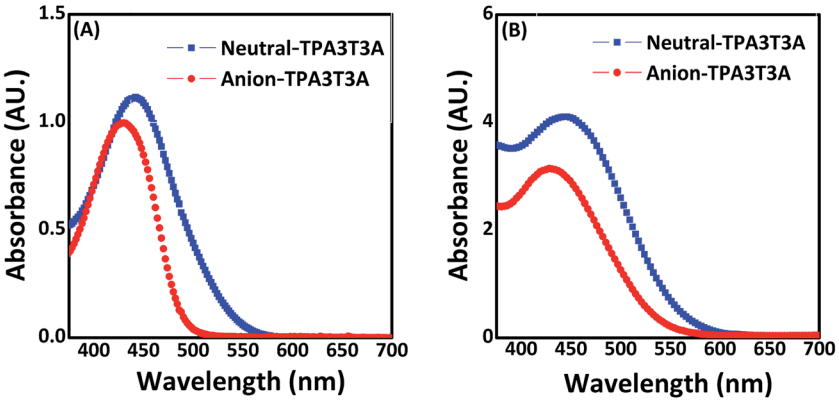

Fig. 3 UV-vis absorption spectra of neutral and anion TPA3T3A in DMF (A) and on the TiO_2 thin films (B).

Table 1 Optical and redox parameters of neutral and anion TPA3T3A sensitizers optical and properties and photovoltaic performance of the DSSCs using neutral and anion TPA3T3A based-sensitizers

Sample	ε_{max} (M^{-1} cm^{-1})	λ_{max} (nm) solution TiO_2	Dye loading (mol cm^{-2})	E_{HOMO} (V)	E_{LUMO} (V)	E_{0-0} (eV)
Neutral-TPA3T3A	79 800	440 444	7.12×10^{-8}	0.87	−1.44	2.31
Anion-TPA3T3A	71 200	429 428	5.49×10^{-8}	0.81	−1.73	2.54

a higher $\varepsilon_{max} = 7.98 \times 10^4$ M^{-1} cm^{-1}. The UV-vis spectrum of the neutral and anion TPA3T3A on the TiO_2 films features a broadened absorption band compared to that recorded in solution, with a clear red shifted maximum (444 *vs.* 440 nm) and a slightly blue shifted maximum (429 *vs.* 428 nm), suggesting a tendency to form J- and H- aggregates on the semiconductor surface, respectively (Fig. 3(B)).[31] A dye loading experiment was carried out by dipping the dye-absorbed TiO_2 films in the mixture solution of 2 M NaOH and DMF (1 : 1 v/v) at 100 °C. The dye loading on the TiO_2 surface of neutral TPA3T3A was 7.12×10^{-8} mol cm^{-2}, which is higher than of anion TPA3T3A, 5.49×10^{-8} mol cm^{-2} (Table 1).

3.3 Electrochemical properties of neutral and anion dyes

The electrochemical characteristics of the neutral and anion TPA3T3A dyes were investigated by means of cyclic voltammetry (CV). The ground and excited state oxidation potentials of the neutral and anion TPA3T3A dyes were measured and the results summarized in Table 1 (for the cyclic voltammograms and schematic energy level diagram of compounds neutral and anion TPA3T3A see Fig. S3†). The ground-state oxidation potentials E_{OX} of neutral and anion TPA3T3A, corresponding to the highest occupied molecular orbital (HOMO) level of dyes, are 0.87 and 0.81 V *vs.* SCE. These values are more positive than the I^-/I_3^- redox potential (0.42 V *vs.* SCE),[32] indicating that there is enough driving force for the dye regeneration. Here, neutral dye has higher energy difference (0.45 V) with the redox potential of I^-/I_3^- than that of anionic TPA3T3A (0.4 V). Therefore, the neutral TPA3T3A can be regenerated more effectively than the anion TPA3T3A. The excited-state oxidation potentials E^*_{OX}, corresponding to the lowest occupied molecular orbital (LUMO) level of dyes, play an important role in the electron injection process. The E^*_{OX} was calculated using: $E^*_{OX} = E_{OX} - E_{0-0}$ where E_{0-0} is the zeroth–zeroth transition value obtained from the onset of absorption spectra in Fig. 3. The LUMO levels of neutral and anion TPA3T3A dye are −1.44 and −1.73 V *vs.* SCE, which are more negative than the conduction band edge of TiO_2 (−0.5 V *vs.* SCE).[32] The driving force is sufficient for efficient charge injection, provided that an energy gap between dye LUMO and TiO_2 conduction band (CB) is >0.2 eV.[15] Thus, the electron injection process from the excited dye molecule to the TiO_2 conduction band and the subsequent dye regeneration are energetically permitted. Such electronic structures thus ensure a favorable exothermic flow of charges throughout the photo-electric conversion.

3.4 Sensitizers and TiO_2 binding properties of neutral and anion dyes

FT-IR spectroscopy was conducted to examine the interaction between the TiO_2 surface and dye molecules, and the results are shown in Fig. 4. In both cases of neutral and anion TPA3T3A, the C≡N signal (~2210 cm^{-1}) appeared in the FTIR spectra of the solid dyes and TiO_2 adsorbed dyes, which indicate no interaction between the cyanide moieties and TiO_2 surface. Fig. 4(A) shows that the signals of the free carboxyl groups of neutral TPA3T3A decreased after absorption on TiO_2 (1713 cm^{-1}) and the symmetrical and asymmetrical stretching band of carboxylate (C=O) were shifted from 1432 cm^{-1} and 1581 cm^{-1} to 1440 cm^{-1} and 1593 cm^{-1}, respectively, after absorption, which suggests that neutral TPA3T3A adsorbs on the TiO_2 surface by both monodentate and bi-dentate binding. In the case of anion TPA3T3A, there is a slightly low-frequency shift of the adsorbed dye compared to the free dye, which indicates that anion TPA3T3A adsorbed on the TiO_2 surface with bi-dentate binding. The bi-

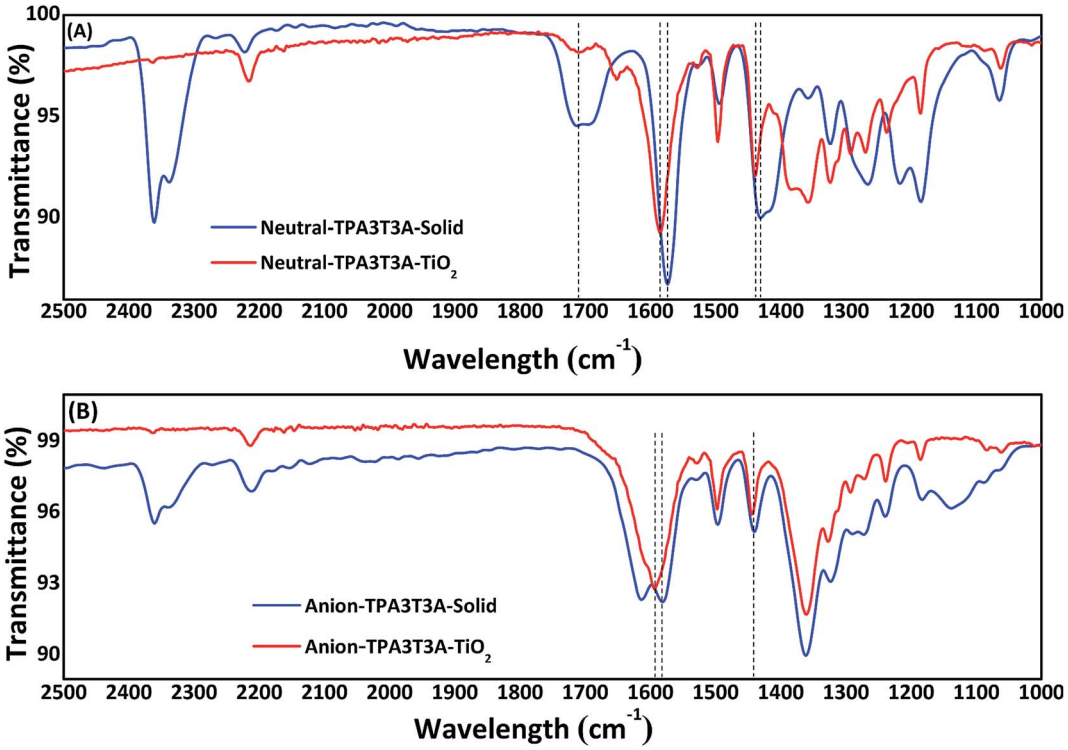

Fig. 4 FTIR spectra of solid state and TiO_2 absorbed neutral (A) and anion (B) TPA3T3A.

dentate binding show easier electron injection from the donor unit triphenylamine to the conduction band of the TiO_2 nanoparticles than mono-dentate.[33–35] However, with bi-dentate binding, anion TPA3T3A reduced the dye loading on the TiO_2 surface, which affects the photovoltaic performance of the DSSCs.

3.5 Influence of neutral and anion adsorption structure on DSSC photovoltaic performance

To investigate the photovoltaic performance of the DSSCs of the neutral and anion TPA3T3A, the current density–voltage (*J–V*) characteristics were examined under the illumination of AM 1.5G solar simulated light (100 mW cm^{-2}). The overall conversion efficiency (η) of a DSSC is determined by the short circuit current density J_{SC} (mA cm^{-2}), open circuit voltage V_{OC} (V), fill factor FF (%) of the cell, and the input irradiation from the light source, P_{in} (mW cm^{-2}).[36]

$$\eta = \frac{J_{SC} \times V_{OC} \times FF}{P_{in}} \quad (1)$$

Fig. 5(A) and Table 2 shows that the neutral TPA3T3A sensitized solar cells produced a J_{SC} of 14.46 mA cm^{-2}, a V_{OC} of 0.593 V and a FF of 0.62, corresponding to a η of 5.27%, and the anion TPA3T3A sensitized devices produced J_{SC}, V_{OC} and FF values of 10.30 mA cm^{-2}, 0.649 V and 0.63, respectively, giving a η value of 4.19%. Anion TPA3T3A exhibited a much higher V_{OC} (0.649 V) than neutral TPA3T3A (0.593 V), which is due mostly to the lower level of proton donation on the TiO_2 surface. Neutral TPA3T3A with a proton (H^+) in the carboxylic group absorbs on the TiO_2 surface, and donates the proton to TiO_2, resulting in a positive shift of the TiO_2 conduction band, which reduces V_{OC} of the DSSC. In contrast, anion TPA3T3A does not contain a proton (H^+), which helps conserve the V_{OC}. Moreover, without a proton, the resonance structure anion TPA3T3A connects to TiO_2 easily by bi-dentate binding, leading to an increase in surface coverage area and resistance between the electrons in TiO_2 and the oxidized electrolyte. Therefore, recombination can be decreased to prevent V_{OC} loss.

Despite the increased surface coverage of anion TPA3T3A reducing recombination the dye loading is reduced compared to neutral TPA3T3A, as mentioned in the previous section. The dye loading of anion TPA3T3A is 5.49×10^{-8} mol cm^{-2}, which is lower than that of neutral TPA3T3A (7.12×10^{-8} mol cm^{-2}), leading to lower J_{SC} and lower photovoltaic performance. Incident photo-to-current conversion efficiency (IPCE) at each incident wavelength was calculated using eqn (2)[37]

$$\text{IPCE} = \frac{1240\ (\text{eV nm}) \times J_{SC}(\text{mA cm}^{-2})}{\lambda(\text{nm}) \times \phi(\text{mW cm}^{-2})} \quad (2)$$

where J_{SC} is the short circuit current density under monochromatic irradiation, λ is the wavelength and ϕ is the power of the incident radiation per unit area.

Table 2 Photovoltaic performance of the DSSCs using neutral and anion TPA3T3A based-sensitizers

Sample	J_{SC} (mA cm^{-2})	V_{OC} (V)	FF (%)	η (%)
Neutral-TPA3T3A	14.46	0.593	61.55	5.27
Anion-TPA3T3A	10.30	0.649	62.78	4.19

Fig. 5(B) presents the maximum quantum efficiency of neutral TPA3T3A (78% at 550 nm), which is higher than that of anion TPA3T3A (61% at 450 nm). The IPCE results show agreement with the short-circuit current density shown in Fig. 5(A).

To further examine the recombination between TiO_2 and the electrolyte, EIS was performed under dark conditions with a bias voltage of −0.7 V over the frequency range, 0.1 Hz to 100 kHz, as shown in Fig. 6. Table 3 lists the extracted parameters, which were fitted by an electrochemical equivalent circuit (Fig. 6) using Z-view software. The electron life time, τ_e, was calculated using eqn 3.[38,39]

$$\tau_e = (R_{rec} \times Q_{rec})^{1/\alpha} \quad (3)$$

where R_{rec} is the recombination resistance between TiO_2 and the electrolyte; Q_{ct} and α is the time constant part and the exponent part of the constant phase element (CPE) between TiO_2 and the electrolyte. The electron lifetime of anion TPA3T3A is 23.05 ms, which is two times higher than that of neutral TPA3T3A, 10.42 ms. The lower electron lifetime of neutral TPA3T3A due to the higher back-recombination rate occurs through electron transfer from TiO_2 to I_3^- at the TiO_2/electrolyte surface. This shows the effective insulation of TiO_2 and electrolyte against electron recombination, resulting in V_{OC} gain in the anion TPA3T3A sensitized solar cells.

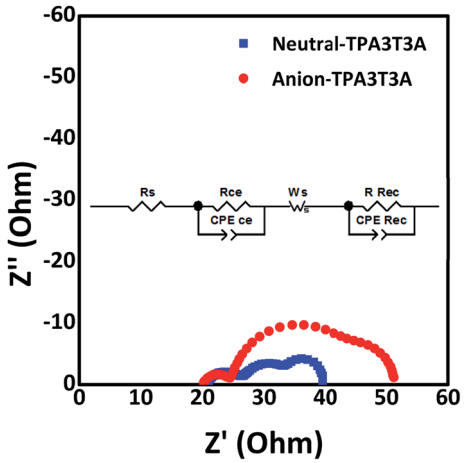

Fig. 6 Nyquist plots of the DSSCs using neutral and anion TPA3T3A based-sensitizers under dark conditions with a bias voltage −0.7 V and (inset) the transmission line model for the DSSCs.

Table 3 EIS parameters and electron life time of the DSSCs containing neutral and anion TPA3T3A-based sensitizers

Sample	R_{rec} (Ω)	Q_{rec} (S s^n)	α	τ_e (ms)
Neutral-TPA3T3A	6.04	0.0025	0.9036	10.42
Anion-TPA3T3A	17.85	0.0017	0.9561	23.05

3.6 Computational studies

DFT/TDDFT calculations were performed to gain further insight into the distinct difference between the structural, electronic and optical properties of neutral and anion TPA3T3A. The optimized structures were compared by overlaying them, as shown in Fig. 7. The structures of the two dyes do not vary to a large extent near the central TPA unit, but a considerable deviation can be seen towards the thiophene and anchoring groups. The electron density distribution in the occupied and virtual molecular orbitals (MO) was obtained from population analysis. Fig. 8 presents the electron density isosurfaces of the neutral and anion TPA3T3A. The neutral and anionic TPA3T3A show a similar electron density distribution pattern in their highest occupied MOs (HOMO). The lowest unoccupied MO's (LUMO) and LUMO+1 of the neutral and anionic TPA3T3A show variations in the electron density distribution. In the HOMO of the two dyes, the electron density is localized mainly over the TPA and thiophene moieties. On the other hand, in the LUMO and LUMO+1, the electron density is shifted towards the anchoring groups. Fig. 8 also shows the optimized geometries of the neutral and anion TPA3T3A. Population analysis calculations were carried out in a DMF solution at the PBE0/6-311G(d,p) level of theory. Fig. 9 presents a schematic diagram

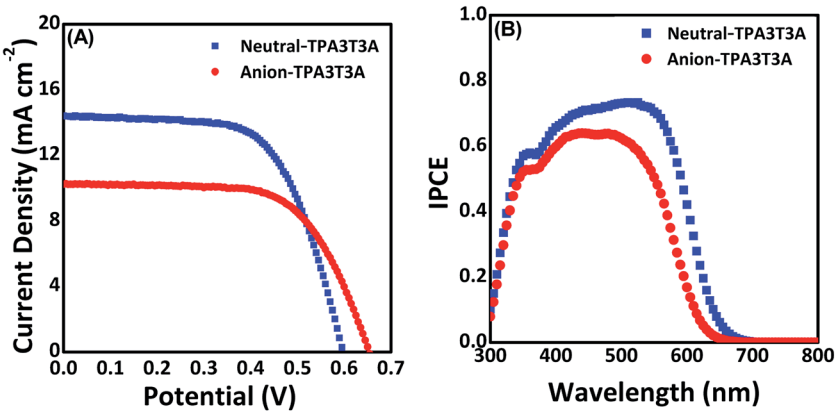

Fig. 5 *J*–*V* characteristics (A) and incident photo-to-current conversion efficiency (IPCE) spectra (B) of the DSSCs using neutral and anion TPA3T3A based-sensitizers under the irradiation of AM 1.5 with an incident power of 100 mW cm^{-2}.

of the obtained Eigen values of the frontier MOs. In the same figure, the energy levels of the two dyes were compared with the conduction band (CB) of the TiO_2 (−4.20 eV) and redox potential (−5.20 eV) of the I^-/I_3^- redox couple. The HOMO energies of the neutral and anionic TPA3T3A were −5.72 and −5.34 eV, respectively. As the HOMO energies of the two dyes are sufficiently low compared to the redox potential of I^-/I_3^-, the oxidized dyes can be regenerated efficiently through the reaction with iodide. Here, the neutral TPA3T3A can be regenerated more effectively than the anion TPA3T3A, because of its higher energy difference (0.52 eV) with the redox potential of I^-/I_3^- than that of anionic TPA3T3A (0.14 eV). This high regeneration of neutral TPA3T3A is also one of the reasons for its high efficiency over anion TPA3T3A. Both the HOMO and LUMO energy levels are up shifted in the transition from neutral TPA3T3A to anion TPA3T3A, but the up shift in the LUMO is higher than in the HOMO, which leads to an increased HOMO-LUMO gap (HLG) of anion TPA3T3A. A considerable hypsochromic shift can be expected for anionic TPA3T3A from neutral TPA3T3A because of the increased HLG. As the LUMO energies of the neutral TPA3T3A (−2.99 eV) and anionic TPA3T3A (−2.21 eV) are well above the CB edge (−4.2 eV) of the TiO_2, the electron from the dye excited state can be injected easily into the nanocrystalline TiO_2. The obtained electronic energy levels of the neutral and anion TPA3T3A dyes showed excellent agreement with the experimental results (Table 1 and Fig. S3†).

The UV-visible absorption spectra of two dyes were then calculated, as shown in Fig. 10, to determine the difference in optical properties between the neutral TPA3T3A and anion TPA3T3A. The first 25 vertical singlet excitations for each dye were calculated in the TDDFT simulations. To mimic the experimental conditions, the TDDFT simulations were performed in a DMF solution using the implicit PCM model. The TDDFT simulations reproduced the main bands that were observed in the experimental UV-visible spectra of the two dyes. The absorption maxima in the low energy region were located at

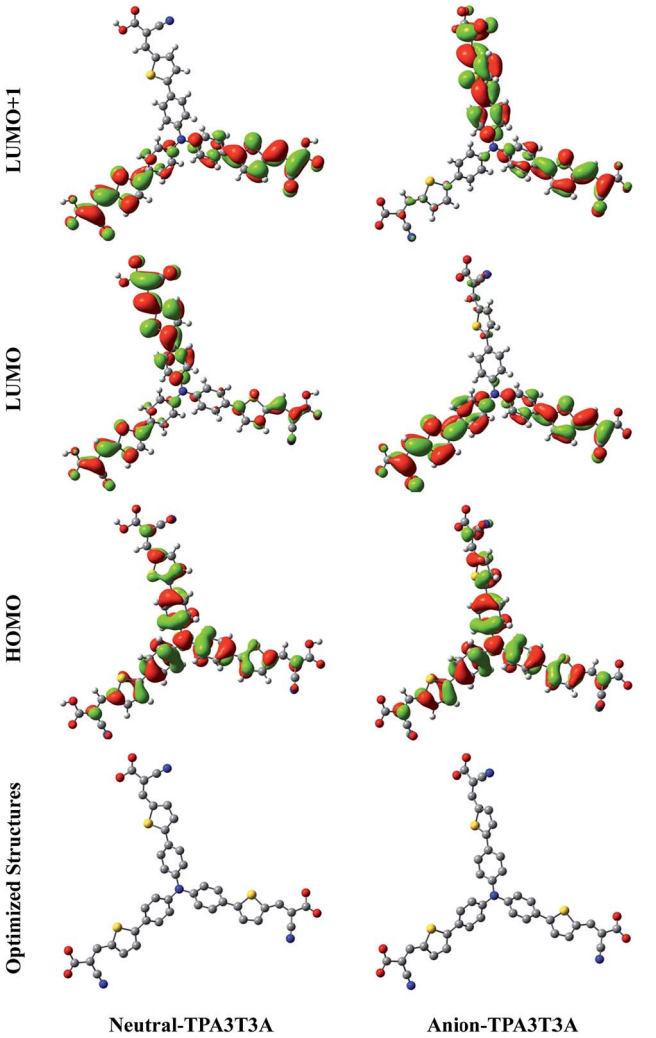

Fig. 8 Ground state optimized geometries and electron density distribution (HOMO, LUMO and LUMO+1) of neutral and anionic TPA3T3A. The hydrogen atoms are omitted in the optimized structures for clarity (isosurface = 0.02 e $Å^{-3}$).

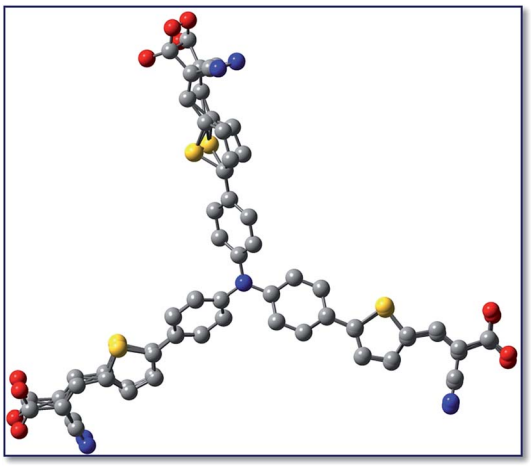

Fig. 7 Overlaid geometries (ball and stick model) of neutral and anion TPA3T3A. The blue, gray, yellow, and red color balls represents nitrogen, carbon, sulfur, and oxygen, respectively. The hydrogen atoms are omitted for clarity.

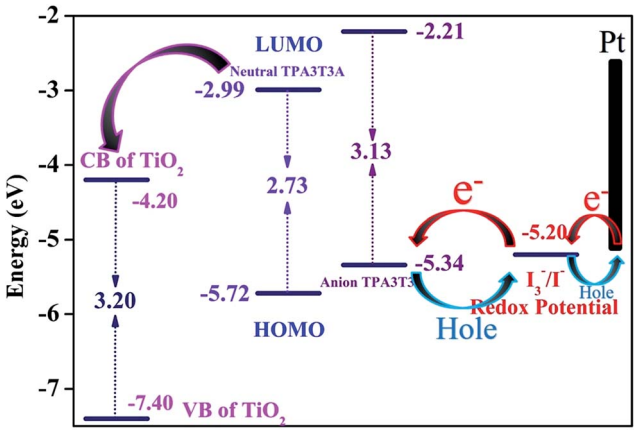

Fig. 9 Schematic energy levels of the neutral and anion TPA3T3A compared to the TiO_2 conduction band edge and redox potential of the redox couple.

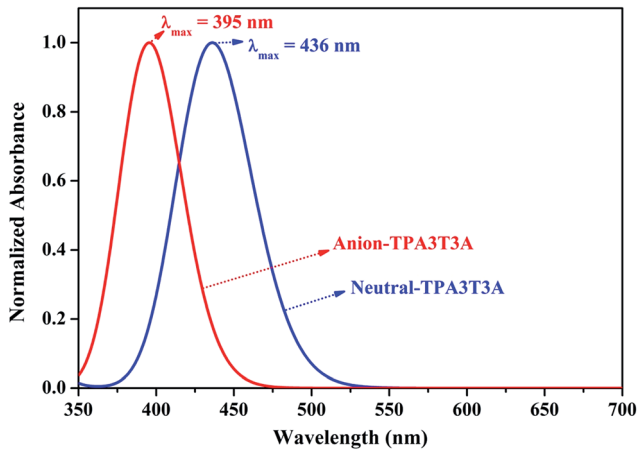

Fig. 10 Simulated UV-vis absorption spectra of the neutral and anion TPA3T3A obtained at the CAM-B3LYP/6-311G(d,p) level of theory.

Table 4 Simulated absorption wavelengths (λ_{cal}), oscillator strengths (f) and coefficient of the configuration interaction (CI) with a dominant contribution to each transition. H and L denote the HOMO and LUMO, respectively

Dye	Transition	λ_{cal} (nm)	f	CI coefficient	Dominant contribution (%)
Neutral	$S_0 \rightarrow S_1$	436	1.7557	0.57620	H → L (66)
	$S_0 \rightarrow S_2$	435	2.1092	0.57407	H → L+1 (66)
	$S_0 \rightarrow S_3$	385	0.0120	0.52759	H → L+2 (56)
	$S_0 \rightarrow S_4$	322	0.2147	0.28388	H-1 → L+2 (16)
	$S_0 \rightarrow S_5$	321	0.1562	0.29102	H-2 → L+2 (17)
Anion	$S_0 \rightarrow S_1$	395	1.9577	0.57515	H → L (66)
	$S_0 \rightarrow S_2$	394	1.9047	0.57420	H → L+1 (66)
	$S_0 \rightarrow S_3$	351	0.0005	0.46911	H → L+2 (44)
	$S_0 \rightarrow S_4$	306	0.0025	0.47070	H-9 → L (44)
	$S_0 \rightarrow S_5$	305	0.0022	0.36197	H-8 → L (26)

436 and 395 nm, respectively, for neutral and anion TPA3T3A. The observed absorption peaks were attributed to the transition from HOMO to LUMO for both dyes. The hypsochromic shift of 41 nm observed for anion TPA3T3A was assigned to the increased HLG. The obtained photophysical properties of the two dyes showed excellent agreement with the experimental results and are summarized in Table 4.

4. Conclusion

Anion TPA3T3A shows the superiority of an increased V_{OC} by protecting the TiO_2 conduction band energy level and reducing recombination due to the greater surface coverage. The neutral TPA3T3A adsorbs on TiO_2 with both mono and bi-dentate binding, whereas anion TPA3T3A interacts with TiO_2 only by bi-dentate binding, which provides efficient electron extraction pathways from the electron donor to TiO_2 and more surface coverage, which can reduce the recombination rate from the TiO_2 surface and oxidized-electrolyte, leading to improved photo-voltage of anion TPA3T3A. On the other hand, the dye loading was reduced. Hence, the decreases in the short-circuit currents and overall energy-conversion efficiencies of anion TPA3T3A are limited (4.19%), which is lower than that of neutral TPA3T3A (5.27%). Therefore, it will be necessary to increase the dye loading of anion dye to enhance the photovoltaic performance of DSSCs. The experimental results are well supported by the theoretical results obtained from the DFT/TDDFT simulations.

Acknowledgements

This work was supported by the 2013 Yeungnam University Research Grant.

References

1 B. O'Regan and M. Grätzel, *Nature*, 1991, **353**, 737–740.
2 M. Grätzel, *Acc. Chem. Res.*, 2009, **42**, 1788–1798.
3 Y. Hou, D. Wang, X. H. Yang, W. Q. Fang, B. Zhang, H. F. Wang, G. Z. Lu, P. Hu, H. J. Zhao and H. G. Yang, *Nat. Commun.*, 2013, **4**, 1583.
4 L.-L. Li and E. W.-G. Diau, *Chem. Soc. Rev.*, 2013, **42**, 291–304.
5 F. F. Gao, Y. Wang, D. Shi, J. Zhang, M. K. Wang, X. Y. Jing, R. Humphry-Baker, P. Wang, S. M. Zakeeruddin and M. Grätzel, *J. Am. Chem. Soc.*, 2008, **130**, 10720–10728.
6 W. Q. Wu, Y. F. Xu, H. S. Rao, C. Y. Su and D. B. Kuang, *J. Am. Chem. Soc.*, 2014, **136**, 6437–6445.
7 S. Mathew, A. Yella, P. Gao, R. Humphry-Baker, B. F. E. Curchod, N. Ashari-Astani, I. Tavernelli, U. Rothlisberger, M. K. Nazeeruddin and M. Grätzel, *Nat. Chem.*, 2014, **6**, 242–247.
8 A. Yella, H.-W. Lee, H. N. Tsao, C. Yi, A. K. Chandiran, M. K. Nazeeruddin, E. W.-G. Diau, C.-Y. Yeh, S. M. Zakeeruddin and M. Grätzel, *Science*, 2011, **334**, 629–634.
9 H. Li, Y. Hou, Y. Yang, R. Tang, J. Chen, H. Wang, H. Han, T. Peng, Q. Li and Z. Li, *ACS Appl. Mater. Interfaces*, 2013, **5**, 12469–12477.
10 Y. Wu and W. Zhu, *Chem. Soc. Rev.*, 2013, **42**, 2039–2058.
11 L. Wang, P. Shen, Z. Cao, X. Liu, Y. Huang, C. Liu, P. Chen, B. Zhao and S. Tan, *J. Power Sources*, 2014, **246**, 831–839.
12 P. Shen, Y. Tang, S. Jiang, H. Chen, X. Zheng, X. Wang, B. Zhao and S. Tan, *Org. Electron.*, 2011, **12**, 125–135.
13 P. Shen, X. Liu, S. Jiang, Y. Huang, L. Yi, B. Zhao and S. Tan, *Org. Electron.*, 2011, **12**, 1992–2002.
14 J. H. Park, B. Y. Jang, S. Thogiti, J.-H. Ryu, S.-H. Kim, Y.-A. Son and J. H. Kim, *Synth. Met.*, 2015, **203**, 235–242.
15 K. S. V. Gupta, T. Suresh, S. P. Singh, A. Islam, L. Han and M. Chandrasekharam, *Org. Electron.*, 2014, **15**, 266–275.
16 A. Hagfeldt, G. Boschloo, L. Sun, L. Kloo and H. Pettersson, *Chem. Rev.*, 2010, **110**, 6595–6663.
17 F. Zhang, F. Shi, W. Ma, F. Gao, Y. Jiao, H. Li, J. Wang, X. Shan, X. Lu and S. Meng, *J. Phys. Chem. C*, 2013, **117**, 14659–14666.
18 F. De Angelis, S. Fantacci, A. Selloni, M. K. Nazeeruddin and M. Grätzel, *J. Am. Chem. Soc.*, 2007, **129**, 14156–14157.
19 F. De Angelis, S. Fantacci, A. Selloni, M. Grätzel and M. K. Nazeeruddin, *Nano Lett.*, 2007, **7**, 3189–3195.

20 C. Bauer, G. Boschloo, E. Mukhtar and A. Hagfeldt, *J. Phys. Chem. B*, 2002, **106**, 12693–12704.
21 F. De Angelis, S. Fantacci, A. Selloni, M. Grätzel and M. K. Nazeeruddin, *Nanotechnology*, 2008, **19**, 424002.
22 L. Q. Bao, N. T. Hai, C. H. Lee, T. Suresh and J. H. Kim, *J. Nanosci. Nanotechnol.*, 2015, **15**, 8813–8819.
23 K. Sodeyama, M. Sumita, C. O. Rourke, U. Terranova, A. Islam, L. Han, D. R. Bowler and Y. Tateyama, *J. Phys. Chem. Lett.*, 2012, **3**, 472–477.
24 C. Anselmi, E. Mosconi, M. Pastore, E. Ronca and F. De Angelis, *Phys. Chem. Chem. Phys.*, 2012, **14**, 15963–15974.
25 N. T. Hai, T. Suresh and J. H. Kim, *Org. Electron.*, 2016, **30**, 40–44.
26 M. J. Frisch, G. W. Trucks, H. B. Schlegel, G. E. Scuseria, M. A. Robb, J. R. Cheeseman, G. Scalmani, V. Barone, B. Mennucci and G. A. Petersson, *et al.*, *Gaussian 09, Revision B.01*, Gaussian Inc, Wallingford, CT, 2010.
27 J. P. Perdew, K. Burke and M. Ernzerhof, *Phys. Rev. Lett.*, 1996, **77**, 3865–3868.
28 C. Adamo and V. Barone, *J. Chem. Phys.*, 1999, **110**, 6158–6169.
29 T. Yanai, D. Tew and N. Handy, *Chem. Phys. Lett.*, 2004, **393**, 51–57.
30 S. Miertuš, E. Scrocco and J. Tomasi, *Chem. Phys.*, 1981, **55**, 117–129.
31 F. C. Spano and C. Silva, *Annu. Rev. Phys. Chem.*, 2014, **65**, 477–500.
32 M. Chandrasekharam, T. Suresh, S. P. Singh, B. Priyanka, K. Bhanuprakash, A. Islam, L. Han and M. Lakshmi Kantama, *Dalton Trans.*, 2012, **41**, 8770–8772.
33 K. E. Lee, M. A. Gomez, S. Elouatik and G. P. Demopoulos, *Langmuir*, 2010, **26**, 9575–9583.
34 C. I. Oprea, P. Panait, J. Lungu, D. Stamate, A. Dumbravs, F. Cimpoesu and M. A. Giruu, *Int. J. Photoenergy*, 2013, **2013**, 893850.
35 C. stern, A. B. Lemeune, Y. Gorbunova, A. Tsivadze and R. Guilard, *Turk. J. Chem.*, 2014, **38**, 980–993.
36 M. K. Nazeeruddin, F. De Angelis, S. Fantacci, A. Selloni, G. Viscardi, P. Liska, S. Ito, B. Takeru and M. Grätzel, *J. Am. Chem. Soc.*, 2005, **127**, 16835–16847.
37 Y. S. Yang, H. D. Kim, J.-H. Ryu, K. K. Kim, S. S. Park, K.-S. Ahn and J. H. Kim, *Synth. Met.*, 2011, **161**, 850–855.
38 J. Bisquert, *Phys. Chem. Chem. Phys.*, 2000, **2**, 4185–4192.
39 G. Xue, X. Yu, T. Yu, C. Bao, J. Zhang, J. Guan, H. Huang, Z. Tang and Z. Zou, *J. Phys. D: Appl. Phys.*, 2012, **45**, 425104–425111.